Catalysis
Science & Technology

RSC Publishing

PAPER

View Article Online
View Journal | View Issue

Cite this: *Catal. Sci. Technol.*, 2013, **3**, 2062

Effects of support pre-calcination on the NO_x storage and reduction performance of Pt–BaO/Al_2O_3 catalysts

Zhun Hu, Wei-Zhen Li, Ke-Qiang Sun* and Bo-Qing Xu*

Received 28th September 2012,
Accepted 9th April 2013

DOI: 10.1039/c3cy00228d

www.rsc.org/catalysis

Effects of the crystalline structure and surface property of the Al_2O_3 support on the NO_x storage and reduction (NSR) performance of Pt–BaO/Al_2O_3 catalysts were studied using catalysts prepared from a series of Al_2O_3 samples obtained by varying the calcination temperature of an $Al(OH)_3$ hydrogel in the range of 450–1000 °C (referred to as the pre-calcination temperature, *PCT*). The texture, crystalline structure and surface acidity of the Al_2O_3(*PCT*) supports were measured employing nitrogen adsorption–desorption, XRD, NH_3-TPD and IR spectroscopy of adsorbed pyridine, respectively. The Al_2O_3(*PCT*) samples showed a gradual ordering of the γ-Al_2O_3 phase when increasing the *PCT* from 450 to 800 °C, and a phase transition from the γ- to θ-Al_2O_3 phase upon further increasing the *PCT* to 1000 °C. The surface density of Lewis acid sites of the Al_2O_3(*PCT*) samples exhibited a maximum at *PCT* in the range of 800–900 °C. The NSR performance of Pt–BaO/Al_2O_3 catalysts derived from the Al_2O_3(*PCT*) samples was studied under cyclic lean/rich conditions. The numbers of NO_x stored and reduced on the Pt–BaO/Al_2O_3(*PCT*) catalysts showed similar volcano-type dependencies on *PCT*, peaking at *PCT* = 800 °C. The origins of the support *PCT* effect were discussed in the light of Pt particle size, the nature of BaO sites and Pt–BaO synergy. It was found that the increase in the crystallinity of the γ-Al_2O_3 phase and the surface acid site density of the supporting Al_2O_3 samples would result in improved proximity and synergy between Pt and BaO sites, leading to much more efficient NSR Pt–BaO/Al_2O_3 catalysts.

1. Introduction

Automobile lean-burn engines operating under oxygen excess conditions could decrease fuel consumption by up to 30% compared to traditional engines working at the stoichiometric air/fuel ratio (A/F) of 14.6, thereby offering encouraging potential in enhancing fuel efficiency and reducing CO_2 emission.[1] However, the presence of excess oxygen in lean exhausts would prevent the reduction of NO_x (NO and NO_2) over the "three-way" catalytic converter optimized for the stoichiometric engines. Therefore, the development of efficient lean NO_x abatement technology remains a challenge to the installation of lean-burn engines in automobiles.

Two of the most promising catalytic technologies to minimize automobile lean NO_x emissions are urea-based selective catalytic reduction (SCR), and cyclic NO_x storage and reduction (NSR, also known as lean NO_x traps).[2] Unlike a SCR catalyst that requires an additional tank for the urea reductant and catalyzes NO_x reduction continuously, a NSR catalyst stores or traps NO_x from the exhausts as nitrates under the lean conditions (usually a few minutes) and uses the unburned engine fuels to reduce the stored NO_x (ideally to N_2) under the rich conditions (usually a few seconds) of the cyclic lean/rich operations of the engines. A NSR catalyst generally consists of an alkali or alkaline earth metal oxide and a precious metal dispersed on a high surface area oxide support. The most typical NSR catalyst has been alumina-supported platinum and barium oxide (Pt–BaO/Al_2O_3),[3,4] in which BaO serves as the component for NO_x storage while Pt plays multiple roles, *i.e.*, catalyze NO oxidation to facilitate NO_x storage under lean conditions, promote the release and reduction of the stored NO_x under rich conditions. Great efforts have been devoted to improve and understand the NSR process of Pt–BaO catalyst. The multicomponent and multifunctional nature of Pt–BaO catalyst dictates that an efficient NSR process would depend not only on the nature of individual BaO and Pt sites but also Pt–BaO interactions which could be critical to their synergy and migration of reaction intermediates.[3–7]

The nature of supporting materials would also strongly affect the NSR performance of Pt–BaO catalyst.[8,9] Many oxides (*e.g.*, ZrO_2, CeO_2, SiO_2, MgO and Al_2O_3) were employed as the support. It was shown that basic supports (*e.g.*, MgO and CeO_2)

Innovative Catalysis Program, Key Lab of Organic Optoelectronics and Molecular Engineering, Department of Chemistry, Tsinghua University, Beijing 100084, China. E-mail: kqsun@mail.tsinghua.edu.cn, bqxu@mail.tsinghua.edu.cn; Tel: +86-10-62789022

were beneficial for the NO_x storage step while acidic supports (*e.g.*, TiO_2 and SiO_2) for the NO_x reduction step. However, γ-Al_2O_3, the most commonly used oxide support, showed the best compromise for both the NO_x storage and reduction steps. Moreover, promoting γ-Al_2O_3 with other metal oxides (such as CoO_x, ZrO_2, CeO_2, and FeO_x) could also significantly improve the NSR performance of Pt–BaO/Al_2O_3 catalysts, as characterized by NO_x storage capacity,[10,11] selectivity to N_2 during the NO_x reduction step[12,13] and/or tolerance to sulphur poison.[14] These remarkable support effects could arise from the fact that support materials affect not only the nature of their supported Pt and BaO but also modulate the Pt–BaO interaction and synergy, which are key to the migration of surface intermediates.[9]

It is well known that γ-Al_2O_3 belongs to the group of defective transition aluminas which contains a series of metastable polymorphs that could be regulated *via* thermal dehydration and dehydroxylation of aluminium hydroxides or oxyhydroxides in the temperature range of 200–1200 °C.[15] Depending on the thermal treatment procedure (temperature program and atmosphere), the development of different metastable polymorphs could also lead to significantly varied texture and surface characteristics in the resultant Al_2O_3 sample. However, little attention has been paid to understand how the properties of Al_2O_3 would affect the NSR performance of Pt–BaO/Al_2O_3 catalysts.

In this work, a series of Al_2O_3 samples are prepared by varying the thermal treatment temperature of the same $Al(OH)_3$ hydrogel in the range of 450–1000 °C (referred to as the pre-calcination temperature, *PCT*), and used to make Pt–BaO/Al_2O_3 catalysts for NSR. The crystallinity and surface properties of these precalcined Al_2O_3 samples are then measured and correlated with the NSR performance of their derived Pt–BaO/Al_2O_3 catalysts. The results lead to new insights into the role of the Al_2O_3 support in the NSR catalysis of Pt–BaO/Al_2O_3 catalysts.

2. Experimental

2.1 Sample preparation

Al_2O_3 support samples were prepared by thermal treatment or pre-calcination at 450–1000 °C in flowing air for 5 h of an $Al(OH)_3$ hydrogel, which was obtained by hydrolysis of $Al(NO_3)_3{\cdot}9H_2O$ (Dongfang Chemical Reagent Company, Beijing) with an aqueous solution of ammonia at pH = 10. The resultant sample was denoted as Al_2O_3(*PCT*) according to the pre-calcination temperature, *PCT*, of the hydrogel.

Pt–BaO/Al_2O_3 catalysts were prepared *via* a two-step wet impregnation method. In the first step, BaO/Al_2O_3 samples were prepared by impregnation of the support material Al_2O_3(*PCT*) with an aqueous solution of $Ba(NO_3)_2$ (Beijing Chemical Reagent Company, Beijing), followed by drying at 60 °C in a rotary evaporator and then calcining in flowing air at 800 °C for 5 h. In the second step, the resultant BaO/Al_2O_3 samples were impregnated with an aqueous solution of $Pt(NH_3)_4(NO_3)_2$ (Alfa), followed by drying at 60 °C in a rotary evaporator and calcining in flowing air at 800 °C for 5 h to prepare the Pt–BaO/Al_2O_3(*PCT*) samples. The loadings of Pt and BaO in these samples were determined to be *ca.* 1.0 wt% and 15.0 wt%, respectively, by X-Ray Fluorescence (XRF) analysis.

2.2 Sample characterization

BET surface areas of the samples were determined from nitrogen adsorption–desorption isotherms at −196 °C on a Micromeritics ASAP 2010C instrument. Prior to the isotherm measurements, the samples were degassed under vacuum at 200 °C.

X-ray diffraction (XRD) patterns were obtained on a Bruker D8 Advance X-ray diffractometer with a Ni-filtered Cu Kα (λ = 0.15406 nm) radiation at 40 kV and 40 mA. Data analysis was performed using JADE (Materials Data, Inc., Livermore, CA). The average crystallite sizes were determined according to the well-known Scherrer equation, $D = 0.90\lambda/\beta\cos\theta$, where θ is the diffraction angle and β the full width at half-maximum (FWHM) of the diffraction peak.

The surface acidity of Al_2O_3(*PCT*) was measured by temperature programmed desorption of NH_3 (NH_3-TPD) and IR spectroscopy of adsorbed pyridine. The NH_3-TPD measurement was conducted on a catalyst analyzer (BEL-A, Japan) with a mass spectrometer (Inprocess Instruments, GAM200) as the detector. The sample (*ca.* 60 mg) was pretreated in a quartz reactor (i.d., 4 mm) with a synthetic air (20 vol% O_2 in Ar) at its *PCT* for 30 min, and then cooled in flowing dry Ar to 100 °C. Adsorption of ammonia was then conducted by switching the reactor to a flow of 1.9 vol% NH_3 in Ar for 30 min. After purging with flowing dry Ar (40 mL min^{-1}) for 40–60 min (until the background signals at m/z = 15, 16 and 17 became stabilized), the reactor temperature was raised to 800 °C at a ramp of 10 °C min^{-1} and the desorption of NH_3 was monitored by recording the signal at m/z = 15 using the mass spectrometer.

IR spectra were recorded using a Perkin-Elmer FT-IR 2000 spectrophotometer in transmission mode at a resolution of 4 cm^{-1}. The samples were pressed into self-supporting wafers (10 mg cm^{-2}), and placed in an *in situ* cell equipped with ZnSe windows. Prior to the IR measurement, each catalyst was pretreated by purging with a flowing synthetic air at 550 °C for 1 h. After cooling to 100 °C, the IR cell was switched to a flowing dry Ar and then a spectrum was recorded as the background after *ca.* 15 min. Pyridine (*ca.* 10 000 ppm) adsorption was conducted for 1 h by making the Ar flow to pass through (bubbling) a pyridine-saturator at 25 °C prior to its entry into the IR cell, followed by purging with flowing dry Ar for 3 h. All the gases are of ultra-pure grade (99.999%), and a possible trace amount of moisture in the flowing gases was eliminated with an ethanol–liquid N_2 trap.

The hydrogen–oxygen titration method[16] was employed to determine the dispersion of Pt. The measurement was carried out on the above-mentioned catalyst analyzer (BEL-A, Japan) at 90 °C. Prior to the measurement, the sample (containing *ca.* 3 mg Pt) was pre-treated at 800 °C for 0.5 h in a flow of 5 vol% H_2 in Ar (30 mL min^{-1}) and then cooled to 90 °C in Ar flow. Pre-oxidation of the sample was performed by switching to a flowing synthetic air for 15 min, followed by purging with a flowing dry Ar. Hydrogen-titration of the adsorbed oxygen was

then conducted by introducing a number of H_2 pulses (0.46 mL per pulse), and the amount of the consumed H_2 was used to calculate the Pt dispersion according to the stoichiometry of the following reactions:[16] $2Pt_s + O_2 \rightarrow 2Pt_s–O$; $2Pt_s–O + 3H_2 \rightarrow 2Pt_s–H + 2H_2O$, where Pt_s denotes a surface Pt site.

2.3 NSR performance and NO_x-TPD measurement

The NSR performance was evaluated using 60 mg of catalyst in a fixed bed plug-flow quartz reactor (i.d., 4 mm) under cyclic lean (1000 ppm NO and 10 vol% O_2 in Ar, 50 min) and rich (1 vol% H_2 in Ar, 15 min) conditions at 300 °C. The total gas flow rate was 40 mL min^{-1}, which corresponds to a gas hourly space velocity of 40 000 mL g^{-1} h^{-1}. The lean/rich switches were intervened by an Ar purge for 5 min. Prior to each test, the catalyst was pretreated in 5 vol% H_2 in Ar at 800 °C for 30 min and then cooled to 300 °C. Collection of the NSR data was made after the catalysts reached their ''steady-performing states'' on a cycle-average basis. The reactor effluent was on-line analyzed using a well-calibrated mass spectrometer (Inprocess instruments, GAM 200) with the following mass-to-charge (m/z) ratios: 2 (H_2), 15 (NH_3), 28 (N_2), 30 (NO, NO_2), 32 (O_2), 40 (Ar), 44 (N_2O) and 46 (NO_2). Time-averaged product selectivity during the rich regeneration phases was given as the material balance according to the numbers of nitrogen atoms in the products (N_2, NH_3 and N_2O).

In some experiments, the sample saturated with NO_x (*i.e.*, at the end of the NO_x storage step) was cooled to 200 °C and then switched to an Ar flow (40 mL min^{-1}) for an *in situ* measurement of temperature programmed desorption of NO_x (NO_x-TPD). The temperature was raised from 200 to 800 °C at a ramp of 10 °C min^{-1}.

3. Results and discussion

3.1 Textural properties of Al_2O_3(*PCT*) samples

The BET surface area, cumulative pore volume and average pore diameter of Al_2O_3(*PCT*) are shown in Table 1. Increasing the *PCT* from 450 to 1000 °C lowered the specific surface area from 414 to 50 m^2 g^{-1}, and the pore volume from 0.38 to 0.20 cm^3 g^{-1}, but increased the average pore diameter from 3.5 to 12.9 nm. Note that these numbers changed abruptly on increasing the *PCT* from 800 to 900 °C.

Table 1 BET surface areas, cumulative pore volumes, average pore diameters and quantified XRD results for Al_2O_3(*PCT*) samples

PCT (°C)	S_{BET} (m^2 g^{-1})	Pore volume (cm^3 g^{-1})	Pore diameter (nm)	$I_{\gamma\text{-}Al_2O_3}$ [a] (a.u.)	$d_{\gamma\text{-}Al_2O_3}$ [b] (nm)	$d_{\theta\text{-}Al_2O_3}$ [b] (nm)
450	414	0.38	3.5	216	4	—
600	316	0.36	4.0	369	5	—
700	196	0.36	5.4	903	6	—
800	160	0.37	6.5	1931	6	—
850	112	0.33	7.1	1754	7	15
900	68	0.24	12.1	1046	—	17
1000	50	0.20	12.9	616	—	21

[a] Intensity of the γ-Al_2O_3 phase was expressed as the height of the diffraction at $2\theta = 37.6°$; the dotted line in Fig. 1 shows the selection of a baseline for the intensity measurements. [b] Estimated according to the Scherrer equation.

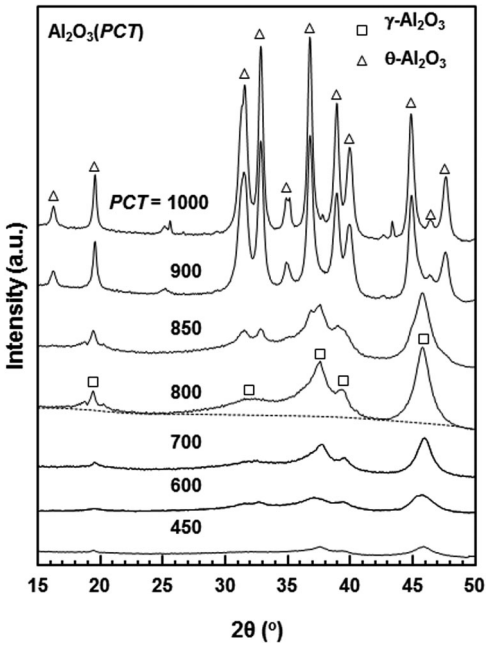

Fig. 1 XRD patterns of Al_2O_3(*PCT*) samples. The dotted line shows how the baseline was determined for measuring the intensity in height of the γ-Al_2O_3 phase at 2θ of 37.6°.

Fig. 1 shows the XRD patterns of Al_2O_3(*PCT*) samples. The weak and broad diffraction peaks at 2θ of 19.5°, 31.6°, 32.7°, 37.5°, 39.5° and 45.7° for the Al_2O_3(450) sample showed the defective spinel characteristics of the γ-Al_2O_3 phase (JCPDS 10-0425). Obviously, these diffractions became sharpened and intensified with increasing *PCT*. The crystallinity of the γ-Al_2O_3 phase was evaluated by measuring the intensity in height of the peak at 2θ of 37.6° according to the baseline exemplified on the pattern for the Al_2O_3(800) sample, and the data are shown in Table 1 for all the Al_2O_3(*PCT*) samples. The intensity of the γ-Al_2O_3 phase for Al_2O_3(600), Al_2O_3(700) and Al_2O_3(800) was enhanced, respectively, to 1.7, 4.2 and 8.9 times that for Al_2O_3(450). When the *PCT* was increased to 850 °C, however, weak features at 2θ of 31.5°, 32.8° and 34.9° were also detectable. These new diffractions developed significantly and three strong ones at 2θ of 36.7°, 38.9° and 44.9° also appeared on further increasing the *PCT* to 900 and 1000 °C, while at the same time the signals for the γ-Al_2O_3 phase became hardly discerned. The intensity in height of the peak at $2\theta = 37.6°$ was lowered from 1931 CPS (the maximum) for the Al_2O_3(800) to 616 CPS for the Al_2O_3(1000) sample.

The crystallization and phase transition sequence of Al_2O_3 during thermal treatment, *i.e.*, boehmite/amorphous $Al_2O_3 \rightarrow \gamma\text{-} \rightarrow \delta\text{-} \rightarrow \theta$-$Al_2O_3$, was originally proposed in the 1960s.[15] However, the existence of the δ-phase was recently questioned.[17,18] A combined XRD, NMR and IR study revealed that the generally taken δ phase was actually a mixture of the γ and θ phases.[18] Accordingly, the new diffractions observed in this current study for the samples of *PCT* > 800 °C would be attributed to the formation of the θ-Al_2O_3 phase (JCPDS 35-0121). The average crystallite sizes of γ- and θ-Al_2O_3 estimated according to the

Scherrer equation are listed in Table 1. The crystallite size of γ-Al_2O_3 measured using the diffraction for the (411) planes at 2θ of 45.7° increased from 4 to 7 nm when the *PCT* was increased from 450 to 850 °C. The crystallite sizes of θ-Al_2O_3 measured using the diffraction for the (200) planes at 2θ of 32.8° were significantly larger, being 15, 17 and 21 nm in the samples of *PCT* = 850, 900 and 1000 °C, respectively (Table 1). Therefore, the present XRD results clearly demonstrate a gradual ordering of the γ-Al_2O_3 phase when the *PCT* was increased from 450 to 800 °C, and a phase transition from γ- to θ-Al_2O_3 when the *PCT* was further increased up to 1000 °C. The variations in the BET surface area, cumulative pore volume and pore diameter between the samples (Table 1) are thus the consequences of the effects of *PCT* on the crystal phase composition and crystallite sizes of Al_2O_3.

3.2 Acidic properties of Al_2O_3(*PCT*) samples

The surface acidity is an important property affecting the catalytic application of transition aluminas. The surface acidity of the Al_2O_3(*PCT*) samples was studied using NH_3-TPD and IR spectroscopy of adsorbed pyridine. The NH_3-TPD curves (Fig. 2) feature a broad peak, starting at *ca.* 150 °C, maximizing at *ca.* 220 °C and lasting up to 600 °C. The increase in *PCT* lowered the intensity but did not obviously alter the overall shape of the TPD peak.

Fig. 3 shows the IR spectra of adsorbed pyridine on Al_2O_3(*PCT*) samples in the region of 1400–1700 cm^{-1}. All of the spectra show bands at 1450, 1490, 1598, 1612 and 1624 cm^{-1}, which are characteristics of the ring vibration modes of adsorbed pyridine coordinating through the nitrogen lone pair to Lewis acid sites (coordinatively unsaturated aluminium cations, Al_{cus}^{3+}).[15] A band at 1578 cm^{-1} was also detected, which would suggest that some pyridine molecules were H-bonded *via* the nitrogen lone pair to surface OH groups.[15] No band due to surface pyridinium ions (*i.e.*, 1540 cm^{-1}) was observed, which is in line with the literature[15,17,18] and indicates that the surface OH groups on Al_2O_3(*PCT*) samples have no sufficient protonic acidity to protonate the pyridine molecules.

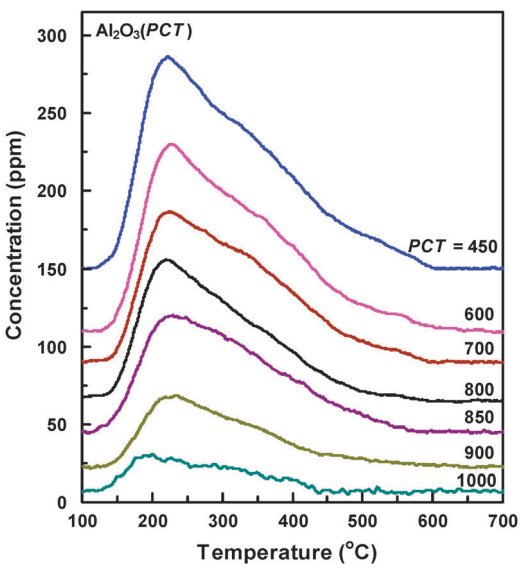

Fig. 2 NH_3-TPD curves of Al_2O_3(*PCT*) samples.

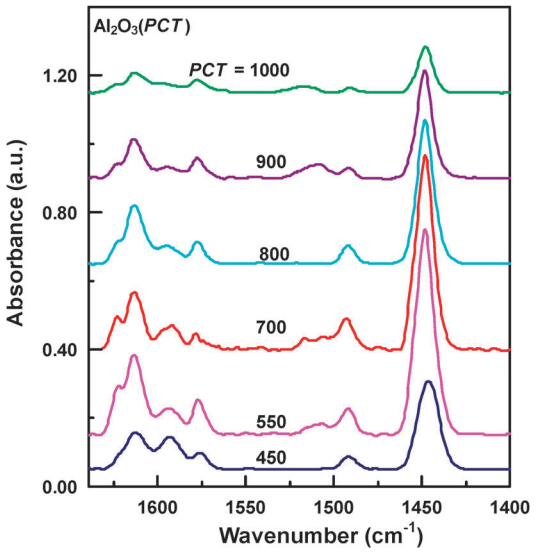

Fig. 3 IR spectra of adsorbed pyridine on Al_2O_3(*PCT*) samples.

The presence of three bands in the region of 1580–1630 cm^{-1} is consistent with the literature,[15,19] indicating the presence of weak (1598 cm^{-1}), medium strong (1612 cm^{-1}) and strong (1624 cm^{-1}) Lewis acid sites. Although some debates exist concerning the exact nature of these acid sites, it was agreed that the acidity of surface Al_{cus}^{3+} sites depends sensitively on their coordination structures, degree of cation vacancy in their coordination sphere.[15,19,20] Note that the shapes of these IR bands and their intensities relative to those of the prominent band at 1450 cm^{-1} varied hardly with the change in *PCT*, which would suggest that the relative amount of the different surface Al_{cus}^{3+} sites on Al_2O_3(*PCT*) did not get obviously perturbed by the variation in *PCT* (at least when *PCT* was no higher than 900 °C). These observations agree with the fact that the phase transition of Al_2O_3 can be regarded as a continuous process, *i.e.*, an ordering of aluminum cations in the lattice of the cubic close packed oxygen anions.[15,17]

Based on the amounts of desorbed NH_3 in NH_3-TPD measurements (assuming one adsorbed NH_3 molecule per acidic site) and the areas of the IR band at 1450 cm^{-1} of adsorbed pyridine, the acidity (amount) and its derived acid site density data normalized to the surface area of the Al_2O_3(*PCT*) samples were obtained (Table 2). The acidity from NH_3-TPD decreased from 0.53 to 0.08 mmol g^{-1} when the *PCT* was increased from 450 to 1000 °C. This trend also agreed with the acidity change estimated from pyridine-IR, with the only exception that the IR measurement of the Al_2O_3(450) sample gave a significantly lower acidity, which was probably arisen from an occurrence of multiple adsorption modes of NH_3 than pyridine.[15] However, the surface densities of acid sites obtained from NH_3-TPD and pyridine-IR spectra showed similar trends with the variation of *PCT*, which increased with *PCT* and peaked when the *PCT* was at 800–900 °C, and then finally decreased when the *PCT* was increased to 1000 °C.

Table 2 Acidity and its acid site density on the surface of Al_2O_3(*PCT*) samples according to NH_3-TPD and pyridine-IR measurements

	Acidity from NH_3-TPD		Acidity from pyridine-IR	
PCT (°C)	Amount (mmol g^{-1})	Density (μmol m^{-2})	Amount (a.u.)	Density (a.u.)
450	0.53	1.28	4.13	0.010
600	0.45	1.44	8.92	0.028
700	0.38	1.93	5.99	0.031
800	0.32	1.98	5.31	0.033
850	0.28	2.51	—	—
900	0.17	2.45	3.58	0.053
1000	0.08	1.58	1.40	0.028

3.3 Textual properties of Pt–BaO/Al_2O_3(*PCT*) samples

The loading of BaO and Pt on Al_2O_3(*PCT*) decreased substantially the specific surface area and the cumulative pore volume but significantly increased the average pore diameter (Table 3). However, the variations of these textual properties with *PCT* were similar to those for the Al_2O_3(*PCT*) supports alone, despite that all the Pt–BaO/Al_2O_3(*PCT*) samples were calcined at the same temperature, *i.e.*, 800 °C. These observations would imply that the *PCT* effect on the textural properties of Al_2O_3(*PCT*) samples is "remembered" by the final Pt–BaO/Al_2O_3(*PCT*) samples.

3.4 NSR performance of Pt–BaO/Al_2O_3(*PCT*) catalysts

The NO_x storage and reduction performance of Pt–BaO/Al_2O_3(*PCT*) catalysts were evaluated according to the cross-cut lean exhaust emission reduction simulations (CLEERS),[21] by using prolonged NO_x storage and reduction cycles employing H_2 as the model reductant.

Fig. 4 shows the effluent concentration profiles of NO_x during the NO_x storage step at 300 °C after the catalysts attained their steady performing states. Upon admitting the NO–O_2 mixture to the reactor, no NO_x could be detected immediately in the effluent, and there was a period of "dead time" before the breakthrough of any NO and NO_2. The duration of the dead time increased from *ca.* 1 to 4 min with increasing the *PCT* of the Al_2O_3 support from 450 to 800 °C, but then turned to decrease to *ca.* 1 min on further increasing the *PCT* to higher temperatures. The concentration of NO_x increased gradually after the breakthrough, and the sum of NO and NO_2 approached that of the inlet NO after 20–25 minutes,

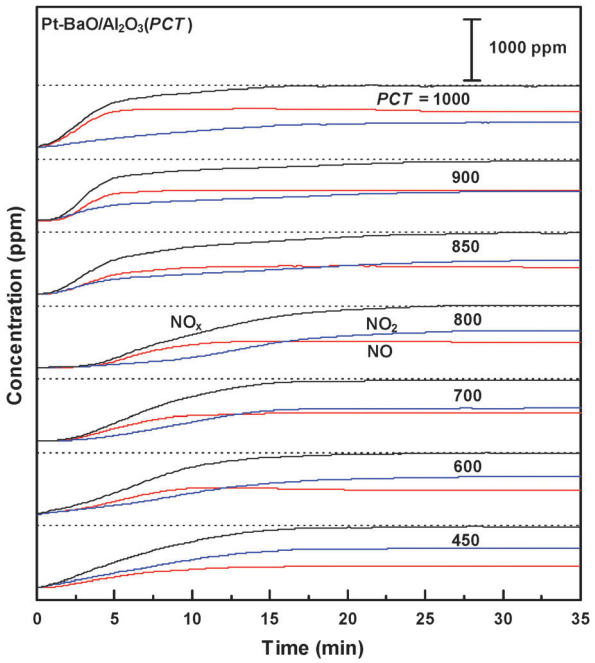

Fig. 4 Effluent concentration profiles of NO_x during the NO_x storage step over Pt–BaO/Al_2O_3(*PCT*) catalysts at 300 °C. The dotted line shows the inlet concentration of NO.

suggesting that the whole catalyst bed was already saturated with the stored NO_x.

The NO_x-saturated Pt–BaO/Al_2O_3(*PCT*) catalysts were then regenerated by reducing the stored NO_x with H_2. Fig. 5 shows the effluent concentration profiles of H_2 and the nitrogen-containing products under the rich conditions. Immediately after switching to the flowing 1 vol% H_2 of the reactor, evolutions of N_2 in 1900–1970 ppm and N_2O in 30–80 ppm were detected. But, the reductant H_2 could not be detected as long as N_2 was in the effluent. The duration for maintaining the high concentration of N_2 (1900–1970 ppm) varied over the Pt–BaO/Al_2O_3(*PCT*) catalysts: it increased from *ca.* 0.7 to 1.5 min when the *PCT* of the Al_2O_3 support was increased from 450 to 800 °C and then decreased to *ca.* 0.7 min on further increasing the *PCT* to 1000 °C. Thereafter, the N_2 concentration decreased steeply to nearly zero. The follow up H_2 breakthrough was always accompanied by an evolution of a small amount of NH_3, which was probably arisen from a Pt-catalyzed H_2-reduction of NO_x under conditions of very high H_2/NO_x ratios. The concentration of H_2 in the effluent then increased quickly to that of the inlet gas (1 vol% H_2), while NH_3 evolved as a broad peak, its maximum concentration varied from 120–200 ppm. The change of the reduction product from N_2 to NH_3 on depletion of the stored NO_x is in good agreement with the observations in the earlier literature.[21–24] Note that no formation of NO and NO_2 was detected during this rich regeneration process.

The amount of stored NO_x measured in the NO_x storage step was referred to as NO_x-storage capacity (NSC), and that of reduced NO_x measured in the NO_x reduction step as NO_x-reduction capacity (NRC). These NSC and NRC data are given in Table 4,

Table 3 Textural property and Pt dispersion of Pt–BaO/Al_2O_3(*PCT*)

PCT (°C)	S_{BET} (m^2 g^{-1})	Pore volume (cm^3 g^{-1})	Pore diameter (nm)	d_{Pt}[a] (nm)	D_{Pt}[b] (%)
450	169	0.39	7.4	28	3.1
600	117	0.28	8.4	30	3.1
700	107	0.25	9.4	30	3.0
800	92	0.20	12.4	31	2.7
850	80	0.20	12.6	31	2.7
900	49	0.20	12.9	32	2.5
1000	43	0.20	12.4	32	—

[a] Estimated by applying the Scherrer equation to the diffraction at $2\theta = 39.8°$. [b] Measured using the hydrogen–oxygen titration method.[16]

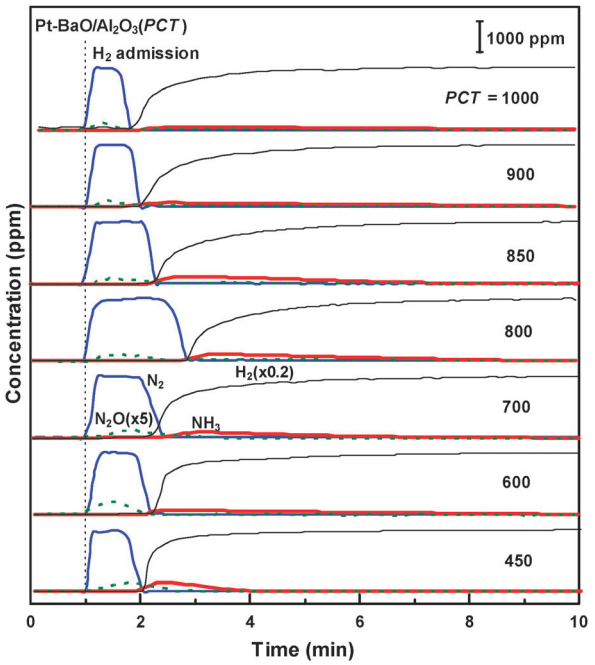

Fig. 5 Effluent concentration profiles of H_2 and the nitrogen-containing products during the NO_x reduction step over the NO_x-saturated Pt–BaO/Al_2O_3(*PCT*) catalysts at 300 °C.

together with the time-averaged product selectivity data calculated according to the effluent concentration profiles during the NO_x reduction step (Fig. 5). The NSC increased from 0.21 mmol g^{-1} for Pt–BaO/Al_2O_3(450), reached a maximum of 0.27 mmol g^{-1} for Pt–BaO/Al_2O_3(800), and then decreased quickly to 0.16 mmol g^{-1} for Pt–BaO/Al_2O_3(1000). On the other hand, the oxidizing capability of the Pt–BaO/Al_2O_3(*PCT*) catalyst, as manifested in Table 4 by the NO_2/NO_x ratio measured after the catalyst was saturated during the NO_x storage step, decreased monotonously with increasing *PCT*.

Similar variations were observed on NRC of the Pt–BaO/Al_2O_3(*PCT*) catalysts: the NRC increased from 0.11 mmol g^{-1} at *PCT* = 450 °C, peaking at 0.23 mmol g^{-1} at *PCT* = 800 °C, and then decreased to 0.09 mmol g^{-1} at *PCT* = 1000 °C. It is not surprising that the number of NSC was always larger than that of NRC, as the intervening Ar purging treatment between the lean/rich alternation would remove those weakly adsorbed NO_x. The product selectivity during reduction of the stored NO_x was essentially the same for all these Pt–BaO/Al_2O_3(*PCT*) catalysts: the selectivity numbers towards N_2, N_2O and NH_3 were around 84%, 3% and 13%, respectively. Clearly, the Pt–BaO/Al_2O_3(800) employing Al_2O_3(800) as the catalyst support showed the best NSR performance.

Table 4 NO_x storage and reduction performance of Pt–BaO/Al_2O_3(*PCT*) catalysts under cyclic lean (1000 ppm NO 10 vol% O_2 in Ar) and rich (1% H_2 in Ar) conditions

	NO_x storage		NO_x reduction			
				Selectivity[d] (N%)		
PCT (°C)	NSC[a]	NO_2/NO_x[b]	NRC[c]	N_2	NH_3	N_2O
450	0.21	0.65	0.11	83.0	13.7	3.3
600	0.22	0.61	0.13	84.2	12.8	3.0
700	0.23	0.55	0.15	83.6	13.2	3.2
800	0.27	0.58	0.23	84.5	14.4	1.1
850	0.21	0.56	0.16	84.3	14.5	1.2
900	0.18	0.50	0.11	87.8	10.6	1.6
1000	0.16	0.42	0.09	88.2	9.9	2.0

[a] NO_x storage capacity (mmol per g-cat) measured under the lean conditions. [b] Fraction of NO_2 in the effluent NO_x after the catalysts became saturated in the NO_x storage step. [c] Amount of nitrogen-containing products (mmol per g-cat) measured under the rich conditions. [d] Time-averaged overall selectivity.

3.5 Origins of the Al_2O_3 *PCT* effect

The catalytic NSR performance would be regarded as the combined result of the intrinsic differential performance and the integral nature of the NSR catalyst in a "plug-flow" reactor.[3] The absence of reactants, *i.e.*, NO_x or H_2, in the effluent at the initial stage of either the NO_x storage or NO_x reduction step was the direct consequence of the integral nature of the NSR process over the present Pt–BaO/Al_2O_3(*PCT*) catalysts. Several NO_x storage and reduction mechanisms over Pt–BaO catalysts have been proposed. The mechanisms for NO_x storages can be roughly classified into two types:[3–7] one is referred to as the "nitrite route" – an oxidative adsorption of NO as surface nitrites is followed by a further oxidation of the adsorbed nitrites to surface nitrates with oxygen or NO_2 spiltover from vicinal Pt; the other is named as the "nitrate route" – NO is oxidized on the Pt sites to NO_2, which then migrates to the active BaO, and finally become stored as nitrates *via* disproportionation ($BaO + 3NO_2 \rightarrow Ba(NO_3)_2 + NO$). The nitrite route generally occurs on BaO sites having intimate contact with Pt (*e.g.*, Pt/BaO interface), and the nitrate route is dominant over those BaO sites far from Pt particles.

For the reduction of the stored NO_x under rich conditions, a Pt-catalyzed surface reaction has been generally accepted.[22–24] Two mechanisms regarding the release of the stored NO_x and its transport from the storing BaO sites to Pt were proposed.[3–7,25,26] The first mechanism suggests a reverse spillover of the stored NO_x from BaO to Pt, which is driven by the scavenging of the oxygen atoms on Pt on admission of the reductant (*e.g.*, H_2 in this work), since the oxidative adsorption of NO_x on Pt–BaO catalyst appears as an equilibrium-driven reaction under the working conditions.[3,25,27] The second mechanism emphasizes the hydrogen spillover from Pt towards the stored nitrate species on the BaO sites and the reduction by the spiltover hydrogen of the nitrates to nitrites, which ultimately results in the release of the stored NO_x.[26]

These mechanisms signify clearly the importance of the properties of Pt for redox catalysis, the transportation of reactive intermediates between the Pt and BaO sites, and a close proximity between the Pt and BaO sites for the NSR process. Moreover, the efficiency of BaO sites for NO_x storage is also a key to the overall NSR performance of Pt–BaO catalyst. Discussion on how these factors would be concerned with the present Pt–BaO/Al_2O_3(*PCT*) catalysts is made below.

3.5.1 Dispersion and particle size of Pt. The catalytic activity of Pt for NO oxidation as well as for NO_x reduction reaction depends critically on the particle size of Pt. Larger Pt particles were found to exhibit higher activity for either NO oxidation or NO_x reduction reaction.[29–31]

The Pt dispersion data for the Pt–BaO/Al_2O_3(*PCT*) catalysts, as measured using the hydrogen–oxygen titration method,[16] are given in Table 3. The dispersion decreased only slightly with the increase in *PCT* of the Al_2O_3 support, from 3.1% for Pt–BaO/Al_2O_3(450) to 2.5% for Pt–BaO/Al_2O_3(1000). Note that these Pt dispersion data are very close to the number (3.2%) measured by CO chemisorption for a Pt–BaO/Al_2O_3 sample calcined at 800 °C,[6] but are significantly lower than those (*e.g.*, 35%) documented for Pt–BaO/Al_2O_3 samples calcined at lower temperatures (*e.g.*, 500 °C).[28]

Powder XRD patterns of the Pt–BaO/Al_2O_3(*PCT*) samples (Fig. 6) were also recorded to estimate the particle sizes of Pt. Besides the diffraction characteristics of γ- and θ-Al_2O_3 crystals, signals featuring metallic Pt at $2\theta = 39.8°$ (JCPDS 04-0802) and $BaAl_2O_4$ crystals at $2\theta = 19.6°$, 28.3°, 34.3°, 40.1° and 41.0° (JCPDS 17-0306) were also clearly detected. The diffraction for metallic Pt ($2\theta = 39.8°$) was extracted from the overlapping signals by careful deconvolution and then used to determine the average particle (crystallite) size of Pt in each Pt–BaO/Al_2O_3(*PCT*) catalyst according to the Scherrer equation. The particle size of Pt increased smoothly from 28 to 32 nm when the *PCT* of the Al_2O_3 support was increased from 450 to 1000 °C (Table 3). These data are in good agreement with the Pt dispersion data (2.5–3.2%) derived from the hydrogen–oxygen titration measurements. Therefore, the essentially unchanged Pt particle sizes should have no direct relation with the volcano-type relationship between NSC (and NRC) and support *PCT* of the Pt–BaO/Al_2O_3(*PCT*) catalysts.

3.5.2 Nature of NO_x storing "BaO" sites. The XRD measurements of Pt–BaO/Al_2O_3(*PCT*) catalysts registered no BaO; the only Ba-containing phase detected was $BaAl_2O_4$ (Fig. 6). This silence of BaO in these XRD patterns is consistent with the earlier documentation[32,33] that BaO particles in NSR Pt–BaO/Al_2O_3 catalysts were sufficiently small and were undetectable by a conventional laboratory powder XRD instrument. With a synchrotron XRD, however, Peden *et al.* were successful in clearly detecting small and broad diffractions featuring BaO crystallites of *ca.* 5 nm.[32] Since $BaAl_2O_4$ was generally regarded as the inert species for NO_x storage,[32,33] the present XRD results fail to provide useful information about the nature of active BaO sites.

To probe the nature of active BaO sites for NO_x storage, NO_x-TPD profiles were measured from Pt–BaO/Al_2O_3(*PCT*) catalysts saturated with NO_x in the NO_x storage step of the cyclic NSR reaction (Fig. 7). The profiles show a NO desorption peak at around 500 °C and a NO_2 desorption peak at around 430 °C. These NO and NO_2 desorptions appeared to be always accompanied by an O_2 desorption, as were reported earlier.[12,32–34] These results would suggest the decomposition of two-type barium nitrate species:

$$4NO_3^- \text{ (surface)} \rightarrow 4NO_2 + O_2 + 2O^{2-} \quad (1)$$

$$4NO_3^- \text{ (bulk-like)} \rightarrow 4NO + 3O_2 + 2O^{2-} \quad (2)$$

Quantification of the TPD peaks is then made according to these two reactions; the results are listed in Table 5. The total amounts of desorbed NO and NO_2 (*i.e.*, D_{NO_x}) were around

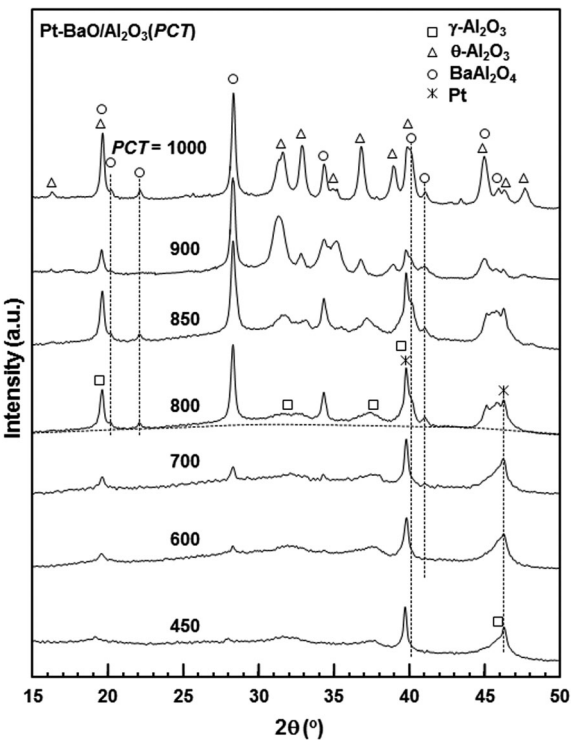

Fig. 6 XRD patterns of Pt–BaO/Al_2O_3(*PCT*) samples.

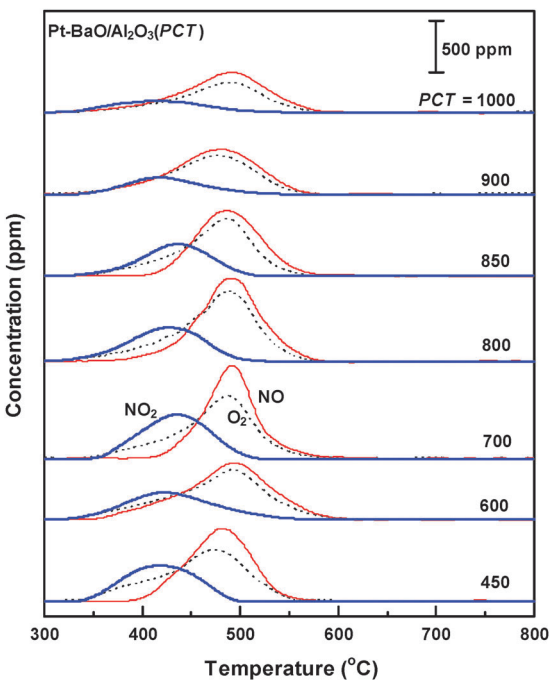

Fig. 7 NO_x-TPD profiles from Pt–BaO/Al_2O_3(*PCT*) catalysts saturated with NO_x in the NO_x storage step.

Table 5 Quantitative NO_x-TPD data of Pt–BaO/Al_2O_3(*PCT*) measured after the NO_x storage step of the cyclic NSR reaction

PCT (°C)	D_{NO_x} (mmol g^{-1})	U_{BaO}[a]	D_{O_2} (mmol g^{-1})	D_{NO}	D_{NO_2}	D_{NO_2}/D_{NO_x}	Density of Ba (atoms per nm^2)
450	0.31	0.14	0.17	0.17	0.16	0.38	3.9
600	0.28	0.12	0.16	0.18	0.10	0.34	5.6
700	0.28	0.13	0.16	0.17	0.11	0.39	6.1
800	0.30	0.14	0.19	0.20	0.10	0.33	7.2
850	0.23	0.10	0.14	0.15	0.08	0.35	8.3
900	0.19	0.09	0.12	0.14	0.05	0.26	13.3
1000	0.17	0.08	0.09	0.13	0.04	0.24	15.2

[a] BaO utilization: fraction of BaO sites actively involved in NO_x storage to all BaO sites, assuming storage of two NO_x molecules per active "BaO" site.

0.30 mmol g^{-1} for Pt–BaO/Al_2O_3(*PCT*) of *PCT* ≤ 800 °C, but decreased to 0.23, 0.19 and 0.17 mmol g^{-1} for the catalysts of *PCT* = 850, 900 and 1000 °C, respectively. Based on the number of D_{NO_x}, the utilization of BaO (U_{BaO}), *i.e.*, the fraction of BaO sites actively involved in NO_x storage to all BaO sites in Pt–BaO/Al_2O_3(*PCT*) catalysts, was calculated assuming that two NO_x molecules were stored per active BaO site.[5,9,11] The number of U_{BaO} remained at around 0.13 for the catalysts with *PCT* ≤ 800 °C but declined to 0.08 when the *PCT* was increased from 800 to 1000 °C. At the same time, the D_{NO_2}/D_{NO_x} ratio, which measures the fraction of active BaO sites at the surface to all of the active BaO sites, remained in the range of 0.33–0.39 for Pt–BaO/Al_2O_3(*PCT*) with *PCT* ≤ 800 °C, but reduced substantially to around 0.25 when the *PCT* was increased to 900 and 1000 °C.

Both the variations of D_{NO_x} and D_{NO_2}/D_{NO_x} with *PCT* of the Al_2O_3 support are indicative of that the dispersion and number of the active BaO sites (involved in the NO_x storage) remained comparable for the Pt–BaO/Al_2O_3(*PCT*) catalysts with *PCT* ≤ 800 °C, but decreased substantially for those with *PCT* ≥ 900 °C, probably due to their significantly lower BaO dispersion as reflected by the density of Ba at the catalyst surface (Table 5).

The dispersion state of BaO strongly affects its NO_x storage capacity. Small BaO particles (*ca.* 5 nm) formed on top of a BaO monolayer were found to exhibit the highest efficiency for NO_x storage while the storage of NO_x on the highly dispersed BaO monolayer was as inefficient as bulky BaO, due to its strong interaction with the alumina surface.[32,35] However, the variation in the dispersion of BaO could not explain why the NRC and NSC changed similarly for all Pt–BaO/Al_2O_3(*PCT*) catalysts (Table 4), hinting that an efficient NO_x reduction catalyst would require a proper synergy between the BaO and Pt sites over the present catalysts.

3.5.3 Pt–BaO synergy and efficiency of NO_x reduction. It is seen that the numbers of D_{NO_x} from the NO_x-TPD measurements (Table 5) were always apparently larger than the NSC and NRC values measured in the lean and rich cycles for every Pt–BaO/Al_2O_3(*PCT*) catalyst (Table 4). This observation would suggest that not all the stored NO_x could be reduced during the present NO_x reduction step under cyclic steady state reaction conditions. To check if the catalyst was free of the stored NO_x after the NO_x-reduction step under the rich conditions, another set of NO_x-TPD measurements were conducted immediately after the NO_x reduction steps. NO_x desorption peaks with shapes similar to, and areas much smaller than those in Fig. 7 were registered, confirming that a considerable percentage (10–20%) of the stored NO_x was leftover and remained unreduced in the catalysts. The incomplete reduction of the stored NO_x on the Pt–BaO/Al_2O_3 catalyst at 300 °C was also observed in the literature, and a complete reduction of the stored NO_x could be achieved when the temperature was higher than 370 °C.[6,35,36]

If the numbers of D_{NO_x} in NO_x-TPD (Table 5) could be regarded as the upper limits that the catalysts could afford for NO_x storage, the NRC/D_{NO_x} ratio would then measure the efficiency of NO_x reduction under the rich conditions. The higher the ratio is, the higher the efficiency of NO_x reduction. The NRC/D_{NO_x} ratio was 0.37, 0.48, 0.57 or 0.77 for Pt–BaO/Al_2O_3(*PCT*) of *PCT* = 450, 600, 700 or 800 °C, but declined to 0.65, 0.58 or 0.53 when *PCT* = 850, 900 or 1000 °C, respectively.

The numbers of NRC and NRC/D_{NO_x} for Pt–BaO/Al_2O_3(*PCT*) catalysts are plotted in Fig. 8 as a function of *PCT*. The XRD intensity of γ-Al_2O_3 ($I_{\gamma\text{-}Al_2O_3}$) in the supporting Al_2O_3 was also incorporated in this figure to gain insight into the effect of *PCT*. Interestingly, the NRC, NRC/D_{NO_x} and $I_{\gamma\text{-}Al_2O_3}$ showed very similar dependences on *PCT* of the Al_2O_3 support, giving similarly shaped volcano-type curves peaking at *PCT* = 800 °C. These correlations would demonstrate that the efficiency of NO_x reduction determines the overall NSR performance of the Pt–BaO/Al_2O_3(*PCT*) catalyst. This is in line with the notion that the reduction of the stored NO_x under rich conditions is the limiting step in the cyclic lean/rich NSR process,[3] and could be further corroborated by the well-observed fact that the NO_x reduction performance is more sensitive than the NO_x storage performance to the Pt loading[12] and/or Pt dispersion[6] as well as the working conditions of the Pt–BaO/Al_2O_3 catalyst.[21,24,36] Moreover, the observed similar dependence of $I_{\gamma\text{-}Al_2O_3}$ on *PCT* reveals again that the crystallinity of γ-Al_2O_3 in the supporting

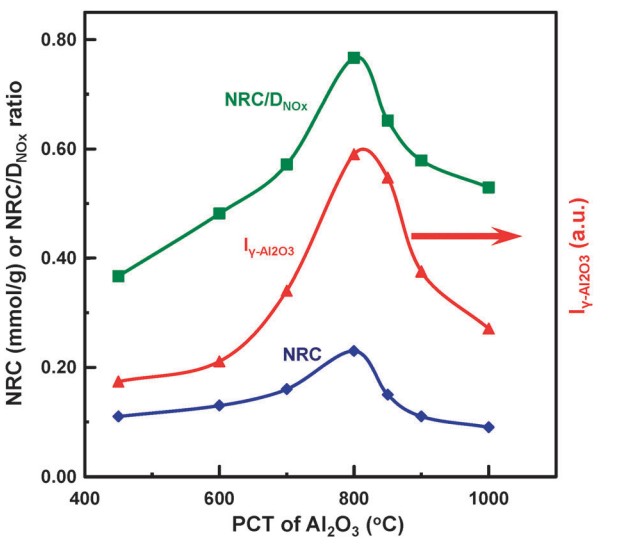

Fig. 8 Dependences of the XRD intensity of the γ-Al_2O_3 phase in Al_2O_3(*PCT*) samples and the NSR performance of the Pt–BaO/Al_2O_3(*PCT*) catalyst on *PCT* of the Al_2O_3 support.

Al_2O_3 should be an important key to the efficiency of NO_x reduction and then the NSR performance of the Pt–BaO/Al_2O_3 catalyst.

The present catalysts were calcined at 800 °C, which led to significant sintering of Pt particles (around 30 nm), or low density of Pt particles (*ca.* 0.2–1.0 Pt particle per million square micrometers). Under such conditions, the synergy between Pt and BaO, *i.e.*, the easiness of spillover of hydrogen and/or NO_x between the catalytic Pt and BaO sites,[6,36] would be very crucial to the reduction of the stored NO_x. As a result, only those NO_x stored on the BaO sites in a reasonable proximity of the catalytic Pt sites could be reduced efficiently, while those stored on BaO sites outside this proximity would be of little accessibility to the reductant (hydrogen in this study) under the rich conditions. The similarity between the three curves of Fig. 8 would therefore imply that the Pt–BaO synergy on the NSR Pt–BaO/Al_2O_3 catalyst could be modulated by changing the crystallinity of γ-Al_2O_3 in the support.

Both BaO and Pt particles would be anchored through some specific sites on the γ-Al_2O_3 surface, such as 5-coordianted Al^{3+} (Al_{cus}^{3+} or Lewis acid sites) as revealed by solid NMR.[37,38] The pyridine-IR measurements of the Al_2O_3(*PCT*) samples (Fig. 3) showed the co-existence of three kinds of Lewis acid sites. These Lewis acidic sites, however, were not detected when we conducted the same (pyridine-IR) measurement with the Pt–BaO/Al_2O_3(*PCT*) catalysts. This annihilation of Lewis acidity gives a further piece of evidence to support that the Lewis acid sites (Al_{cus}^{3+}) on the alumina support served as the anchoring sites for Pt and BaO. Therefore, the proximity between these anchored Pt and BaO would be dependent on the density of Al_{cus}^{3+} at the surface of Al_2O_3; this explains why the *PCT* of the Al_2O_3 support would impact the Pt–BaO synergy and NSR performance of Pt–BaO/Al_2O_3 catalysts.

An attempt is made in Fig. 9 to correlate the NRC numbers with the acid site density measured from NH_3-TPD, which identifies two straight lines. The catalysts prepared from the supports containing crystallites only in the γ-Al_2O_3 phase (*i.e.*, at *PCT* ≤ 800 °C) are linked by the upper line, while the other catalysts prepared from those supports containing crystallites mainly in the θ-Al_2O_3 phase or in mixed γ- and θ-Al_2O_3 phases (*i.e.*, at *PCT* > 800 °C) by the lower line. An important relationship between the catalyst's NRC and the acid site density on the support surface is demonstrated by both lines, *i.e.*, the higher the acid site density on the Al_2O_3 sample, the higher the NRC of its derived Pt–BaO/Al_2O_3 catalyst. Correlating the efficiency of NO_x reduction (*i.e.*, NRC/D_{NO_x}) with the acid site density on the support has produced similar correlations (not shown).

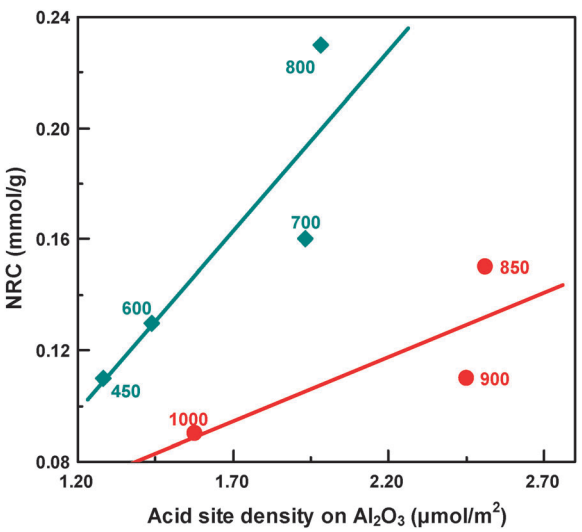

Fig. 9 Correlation of the NSR performance of Pt–BaO/Al_2O_3(*PCT*) catalysts with the acid site density on the Al_2O_3 support. The numbers besides the data points denote the specific support *PCT* for each individual catalyst.

The above discussion indicates that the effect of *PCT* on the NSR performance of the Pt–BaO/Al_2O_3(*PCT*) catalysts could be traced back to the crystallinity and surface acid site density of the Al_2O_3 support. The increase in the density of surface Lewis acid sites on the Al_2O_3 support would result in increased density of Pt and BaO particles in the catalyst, leading to more properly sized BaO particles residing in the proximity of the redox Pt sites or shortened distance between the Pt and BaO sites and therefore more efficient transfer of reaction intermediates between these two kinds of active sites.

The lower position and smaller slope of the line linking the catalysts prepared from the supports with dominating θ-Al_2O_3 (Fig. 9) would suggest that as the support of the NSR Pt–BaO catalyst, Al_2O_3, in the θ-phase is inferior to its counterpart in the γ-phase. This would be partly due to that Al_2O_3 in the θ-Al_2O_3 phase was formed as much larger particles (at *PCT* > 800 °C) and has much smaller specific surface area (Table 1), over which more bulky BaO entities would be easily produced. On the other hand, the surface properties of the Al_2O_3 support would change profoundly as a consequence of the phase transition from the γ- to θ-phase (at *PCT* > 800 °C), which might lead to significant violation to the Pt–BaO synergy for NSR. These explanations are of course not exhaustive, further study is required to understand the effects of crystallite structure and surface property of transition aluminas on the proximity of Pt–BaO and the migration of surface NO_x and hydrogen species.

4. Conclusions

Our data demonstrate that the NSR performance of Pt–BaO/Al_2O_3 catalysts depends strongly on the *PCT*, pre-calcination temperature, of $Al(OH)_3$ during preparation of the Al_2O_3 support. The numbers of NO_x stored and reduced during the cyclic NSR process on the Pt–BaO/Al_2O_3(*PCT*) catalysts showed similar volcano-type dependences on the *PCT*, peaking at *PCT* = 800 °C. The gradual evolution and ordering of the γ-Al_2O_3 phase in the Al_2O_3(*PCT*) support on increasing the *PCT* up to 800 °C led to continued increases in the acid site density at the support surface, which in turn resulted in improved proximity and synergy between the Pt and BaO sites for much more efficient NSR catalysis. These results reveal that both the crystallinity of the γ-Al_2O_3 phase and Lewis acidity of the Al_2O_3 support are critical to the NSR efficiency of the Pt–BaO/Al_2O_3 catalyst.

Acknowledgements

The authors wish to thank National Natural Science Foundation of China (grant: 20703028, 20921001 and 21173214) for providing a financial support of this work.

Notes and references

1 R. M. Heck and R. J. Farrauto, *Catalytic Air Pollution Control*, Van Nostrand-Reinhold, New York, 1995.
2 N. Miyoshi, S. Matsumoto, K. Katoh, T. Tanaka, J. Harada, N. Takahashi, K. Yokota, M. Sugiura and K. Kasahara, SAE Technical Paper Series, 1995, 950809.
3 W. S. Epling, L. E. Campbell, A. Yezerets, N. W. Currier and J. E. Parks, *Catal. Rev.*, 2004, **46**, 163.
4 S. Roy and A. Baiker, *Chem. Rev.*, 2009, **109**, 4054.
5 I. Nova, L. Lietti, L. Castoldi, E. Tronconi and P. Forzatti, *J. Catal.*, 2006, **239**, 244.
6 R. D. Clayton, M. P. Harold, V. Balakotaiah and C. Z. Wan, *Appl. Catal., B*, 2009, **90**, 662.
7 N. W. Cant, I. O. Y. Liu and M. J. Patterson, *J. Catal.*, 2006, **243**, 309.
8 K. Shimizu, Y. Saito, T. Nobukawa, N. Miyoshi and A. Satsuma, *Catal. Today*, 2008, **139**, 24.
9 N. Maeda, A. Urakawa and A. Baiker, *J. Phys. Chem. C*, 2009, **113**, 16724.
10 R. Vijay, C. M. Snively and J. Lauterbach, *J. Catal.*, 2006, **243**, 368.
11 Z. Hu, K.-Q. Sun, W.-Z. Li and B.-Q. Xu, *Catal. Today*, 2010, **158**, 432.
12 W.-Z. Li, K.-Q. Sun, Z. Hu and B.-Q. Xu, *Catal. Today*, 2010, **153**, 103.
13 N. Le Phuc, X. Courtois, F. Can, S. Royer, P. Marecot and D. Duprez, *Appl. Catal., B*, 2011, **102**, 362.
14 P. N. Lê, E. C. Corbos, X. Coutois, F. Can, S. Royer, P. Marecot and D. Duprez, *Top. Catal.*, 2009, **52**, 1771.
15 C. Morterra and G. Magnacca, *Catal. Today*, 1996, **27**, 497.
16 J. Dawody, L. Eurenius, H. Abdulhamid, M. Skoglundh, E. Olsson and E. Fridell, *Appl. Catal., A*, 2005, **296**, 157.
17 M. Trueba and S. P. Trasatti, *Eur. J. Inorg. Chem.*, 2005, 3393.
18 C. Pecharromán, I. Sobrados, J. E. Iglesias, T. González-Carreño and J. Sanz, *J. Phys. Chem. B*, 1999, **103**, 6160.
19 X. Liu and R. E. Truitt, *J. Am. Chem. Soc.*, 1997, **119**, 9856.
20 G. Busca, V. Lorenzelli, V. Sanchez Escribano and R. Guidetti, *J. Catal.*, 1991, **131**, 167.
21 W. S. Epling, A. Yezerets and N. W. Currier, *Appl. Catal., B*, 2007, **74**, 117.
22 L. Lietti, I. Nova and P. Forzatti, *J. Catal.*, 2008, **270**, 257.
23 S. S. Mulla, S. S. Chaugule, A. Yezerets, N. W. Currier, W. N. Delagass and F. H. Ribeiro, *Catal. Today*, 2008, **136**, 136.
24 I. Nova, L. Castoldi, L. Lietti, E. Tronconi and P. Forzatti, *Top. Catal.*, 2007, **42/43**, 21.
25 Z. Liu and J. A. Anderson, *J. Catal.*, 2004, **224**, 18.
26 J. Coronado and J. Anderson, *J. Mol. Catal. A: Chem.*, 1999, **138**, 83.
27 J. P. Breen, C. Rioche, R. Burch, C. Hardacre and F. C. Meuner, *Appl. Catal., B*, 2007, **72**, 178.
28 B. Pereda-Ayo, D. Divakar, R. López-Fonseca and J. R. González-Velasco, *Catal. Today*, 2009, **147S**, S244.
29 L. Olsson, B. Westerberg, H. Persson, E. Fridell, M. Skoglundh and B. Andersson, *J. Phys. Chem. B*, 1999, **103**, 10433.
30 S. S. Mulla, N. Chen, L. Cumaranatunge, G. E. Blau, D. Y. Zemlyanov, W. N. Delgass, W. S. Epling and F. H. Ribeiro, *J. Catal.*, 2006, **241**, 389.
31 R. Burch and P. J. Millington, *Catal. Today*, 1995, **26**, 185.
32 T. Szailer, J. H. Kwak, D. H. Kim, J. Szanyi, C. M. Wang and C. H. F. Peden, *Catal. Today*, 2006, **114**, 86.
33 W.-Z. Li, K.-Q. Sun, Z. Hu and B.-Q. Xu, *Catal. Lett.*, 2009, **132**, 189.
34 N. W. Cant and M. J. Patterson, *Catal. Today*, 2002, **73**, 271.
35 M. Piacentini, M. Maciejewski and A. Baiker, *Appl. Catal., B*, 2005, **59**, 187.
36 N. Le Phuc, X. Courtois, F. Can, S. Royer, P. Marecot and D. Duprez, *Appl. Catal., B*, 2011, **102**, 353.
37 J. H. Kwak, J. Z. Hu, D. H. Kim, J. Szanyi and C. H. F. Peden, *J. Catal.*, 2007, **251**, 189.
38 J. H. Kwak, J. Hu, D. Mei, C. W. Yi, D. H. Kim, C. H. F. Peden, L. F. Allard and J. Szanyi, *Science*, 2009, **325**, 1670.